JOURNAL OF MATERIALS SCIENCE 21 (1986) 3455–3466

Boron modification of carbon fibres

A. AGRAWAL, H. YINNON, D. R. UHLMANN
Department of Materials Science and Engineering, Massachusetts Institute of Technology, Cambridge, Massachusetts 02139, USA

ROGER T. PEPPER
Fiber Materials Inc, Biddeford, Maine 04005, USA

C. R. DESPER
Army Materials and Mechanics Research Center, Watertown, Massachusetts 02172, USA

An investigation is reported of the effect of boron modification on the mechanical properties of carbon fibres. It was found that the presence of boron in the furnace atmosphere does not affect the important structural features of the bulk of the fibres, that in many fibres the added boron is largely confined to the near-surface regions of the fibres, and that a large fraction of the boron is present as boron carbide. The largest improvements in strength were obtained when both carbon and boron were present in the furnace atmosphere.

1. Introduction

The maximum theoretical modulus for single crystal graphite is approximately 140 × 10^6 psi,* and the theoretical strength is correspondingly about 14 × 10^6 psi normal to the *c*-axis. In commercial carbon fibres, however, the idealized graphitic structure is not developed. In such fibres, the *c*-axis spacing between the layers is larger; and the basal planes are oriented randomly with respect to one another, while remaining largely parallel. Hence even high-performance carbon fibres achieve only about half of the theoretical modulus and a very small fraction of the theoretical strength. Many reasons have been cited for these discrepancies. Most prominently cited is the fact that carbon fibres are not single crystals and have numerous morphological and surface flaws.

Analyses of the fracture of carbon fibres have shown that both internal and surface flaws are responsible for the severe reduction of strength from theoretical values (e.g. [1–5]). Elimination of the internal and external flaws leads to an improvement in the strength of carbon fibres [1, 6].

1.1. Effects of boron additions

Recognition that metal or mineral additions can favourably influence the graphitization process has been used [7–9] to transform a thermally non-graphitizable carbon material into a well-ordered graphite. The heat-treatment temperature required to effect such a transformation in thermally graphitizable materials could also be reduced. As summarized by Weisweiler *et al.* [10], such catalytic graphitization takes place by the dissolution of disordered carbon by the metal, metal carbide or metal boride up to the limit of solubility. Since graphite is the most highly ordered form of carbon, it is expected that the metal, when saturated with respect to the disordered carbon, will be supersaturated with respect to graphite. This is in accord with the reaction mechanism originally suggested by Gillot [11].

Yokokawa [12, 13] suggested another mechanism for the graphitization of carbons from resins with three-dimensionally cross-linked structures. These carbons would have well-developed condensed aromatic clusters that are amorphous and extremely resistant to graphitization. The catalyst should be capable of cleaving the cross links between the aromatic rings by the formation of an intermediate. On this basis, any metal or metal carbide posssessing a considerable solubility for carbon should be a suitable catalyst for graphitization. Metals having the tendency to form carbides can also act as catalysts provided the temperature of the heat lies above the melting point of the carbide [10].

Boron exhibits strong catalytic influences on this process [9, 14, 15]. For boron, the free energy of formation of carbide is negative at 2340° C, and this should favour carbide formation. At such graphitization temperatures, the carbide is molten and could act as a catalyst [10]. Not every form of boron would be equally effective in catalysing the reaction, as illustrated by the fact that B_4C is much more effective than B_2O_3 [16].

The maximum degree of graphitization is reached at about 1% boron content, for simultaneously deposited pyrolytic boron and graphite [17, 18]. This has been attributed to the maximum substitutional solubility of boron. There is a consensus among different workers on the effects brought about by susbtitutional boron, but not on the maximum solubility of boron in the carbon matrix.

Work on pyrolitic graphite [19] has indicated a marked improvement in strength and hardness upon introducing boron during the chemical vapour

*10^3 psi = 6.89 N mm^{-2}.

0022–2461/86 $03.00 + .12

TABLE I

	Graphitization temperature (° C)	Strength (10^3 psi)	Modulus (10^6 psi)	Density (g cm^{-3})
8 to 10 μm diameter pitch fibre (VSB-64)†	2360	258	68.4	2.07
Meradcom/FMI 3 μm diameter PAN-based fibre	2360	448	64.4	1.94

*Graphitization conducted in triethylborane/methane/hydrogen atmosphere.
†Trade marke of the Union Carbide Corporation.

deposition of graphite. Ezekiel [20] has shown that boron additions of 0.1 to 1% dramatically increase the rate of graphitization of carbon fibres. He obtained increases in modulus as large as 300% and in strength as large as 50% compared with fibres treated under the same conditions without boron. X-ray diffraction results showed that the boron-doped fibres had a more axial orientation, were more crystalline, and had smaller interlayer spacings than the undoped fibres. Allen *et al.* [21] also reported an increase in modulus of boron-doped carbon fibres.

Work by Pepper *et al.* [22] has indicated that boron treatment increases significantly both the tensile strength and modulus of carbon fibres. As an example, for a graphitization temperature of 2300° C, small diameter undoped fibres had elastic moduli in the range 45 to 49 $\times$ 10^6 psi and tensile strengths in the range of 250 to 350 $\times$ 10^3 psi. By comparison, boron-treated fibres graphitized at the same temperature had moduli in the range of 55 to 65 $\times$ 10^6 psi and tensile strengths of 400 to 500 $\times$ 10^3 psi.

A comparison of the properties of the small diameter boron-treated PAN-based fibres with larger diameter pitch-based fibres is shown in Table I [22]. It is noted that boron-treated PAN-based fibres provide higher strength at a given level of modulus and lower density than the pitch-based fibres.

Despite the attractiveness of high-temperature boron treatment of carbon fibres, and despite the general qualitative consensus on the catalytic effects of boron on the graphitization process, the correlation between results obtained by different investigators is often poor. More importantly, there is no agreement on the effects of processing conditions employed (the form of boron used, the concentration of boron, and the heat-treatment temperature) on the morphology and properties of the product from similar precursors. Furthermore, almost nothing is known about the detailed mechanism by which boron affects the mechanical properties of carbon fibres. Of particular interest in this regard is the finding of Pepper *et al.* [22] that chemical analysis of a number of boron-treated fibres failed to detect the presence of boron.

The present investigation was undertaken to clarify these questions, and to provide insight into the role of boron in the furnace atmosphere in affecting the characteristics of the resulting carbon fibres.

2. Fibres investigated

The present investigation was concerned with PAN-based carbon fibres which were subjected to a number of graphitization treatments, with varying concentrations of boron in the atmosphere of the graphitization furnace. The specific fibres studied, as well as their mechanical properties when available, are listed in Table II. Fibres prefixed as FMI were supplied by

TABLE II Carbon fibres studied, conditions of their processing (when known), and their mechanical properties

Sample	Temperature (° C)	Atmosphere	B/C ratio	UTS (10^3 psi)	E (10^6 psi)	Denier (g 9000 m^{-1})	Density (g cm^{-3})	Comments
107-74	2300	Ar	NA	*	*	2041	1.80	
098-374	2300	Ar, TEB, H_2	1:6	400	60	1550	1.96	
107-74A (2 runs)	1:2300 2:2300	Ar Ar	NA NA	*	*	2156	1.80	Fibre from run no. 1 was used for run no. 2
107-74B (2 runs)	1:2300 2:2300	Ar Ar, TEB, H_2	NA1:6	*	*	2364	1.83	Fibre from run no 1 was used for run no. 2
098-85	2300	N_2	NA	339	48.8	2138	1.77	
098-87	2300	N_2, B_2H_6	NA	319	50.6	2189	1.80	
098-89	2300	N_2, B_2H_6, CH_4	1:1.5	372	51.6	2202	1.81	
098-91	2300	N_2, B_2H_6, CH_4	1:2.7	372	49.9	2263	1.80	
098-93	2300	N_2, B_2H_6, CH_4	1:7.4	363	45.3	2385	1.82	
16-2	2300-2350	N_2, B_2H_6, CH_4	1:1.5	302	57.8	1172	1.88	Residence time 3 times as compared to run no. 21-4, 19-2, and 21-8
21-4	2300-2350	N_2, B_2H_6, CH_4	1:1.5	364	57.3	1220	1.86	
19-2	2300-2350	N_2, B_2H_6, CH_4	1:2.5	418	58.8	1301	1.86	
21-8	2300-2350	N_2, B_2H_6, CH_4	1:6.5	473	60.3	1309	1.81	
Avco G-160				425	32		1.75	
HMS				324	51.1		1.83	
AS4				516	34		1.80	
HMPVA				360	50.2		1.81	

Fiber Materials Inc. Fibres HMS, HMPVA and AS4 were manufactured by Hercules Inc. HMPVA is made from the same precursor as the FMI fibres, but the latter have about two times the draw ratio. The last specimen was supplied by Avco Inc.

The precursor of the FMI fibres was oxidized in the presence of air and stretched to about 300%. Carbonization was carried out from 300 to 900° C in a nitrogen atmosphere for 8 min at 0% stretch. Another carbonization treatment was given at 1400° C for 1 min. Graphitization was carried out at 2300° C. Both AS4 and Avco are high strength, low modulus fibres.

3. Experimental procedures

The experimental techniques employed to characterize the structure of the fibres were: scanning electron microscopy; transmission electron microscopy; wide-angle X-ray diffraction; small-angle X-ray scattering; Auger electron spectroscopy; X-ray photoelectron spectroscopy.

3.1. Scanning electron microscopy (SEM)

The fibres were examined for their surface texture, both external surfaces and fracture surfaces, using Joel JSM-35, Amray AMR 1000A and ISI DS 130 scanning electron microscopes. Fracture surfaces were generated by impregnating strands of the carbon fibres with Epon 812 epoxy resin, curing the resin, and breaking the specimens with a tensile testing machine at a strain rate of 0.1 sec^{-1}. In some cases, fracture surfaces from tensile tests were recovered and supplied to us by FMI. Polished specimens were made by embedding yarns in a low viscosity epoxy resin. After curing the resin, the specimens were polished using 0.3 μm alumina followed by ultrasonic cleaning. Etching was carried out by argon and air plasmas. Initially radio frequency reverse-sputtering equipment with an argon plasma was used; but there were indications of redeposition of the material from the sample holder and the matrix and some other components of the instrument. Later a plasma stripper made by Process Control Division (PDS-302) was used.

3.2. Transmission electron microscopy (TEM)

Most of the TEM studies were conducted on a Phillips EM 300 or Siemens Elmiskop 101 electron microscopes. Specimens were embedded in an epoxy resin, following the technique reported elsewhere [23]. The samples were microtomed using an LKB Ultramicrotome with both diamond and glass knives. It was observed that cutting the fibres longitudinally was easier and gave more uniform sections than cutting through the cross sections. Some specimens were prepared by grinding the fibres as suggested by Johnson and Crawford [24].

3.3. Wide-angle X-ray diffraction

Initial experiments were carried out on a Debye Scherrer camera with a Gandolfi attachment to get an estimate of the type and intensities of the reflections present. Only the reflections of the type (0 0 2) were intense enough for meaningful interpretation. The samples were then examined in detail on a diffractometer to determine the positions and widths of the (0 0 2) reflection. The fibre axis was oriented perpendicular to the plane containing the incident and the diffracted beams. Transmission X-ray diffraction runs on thin strands were done using a Xentrics/Wicat system. Similar data as obtained from the diffractometer runs were generated. In addition, azimuthal scans of (0 0 2) arcs were made to determine the orientation of the basal planes.

3.4. Small-angle X-ray

The nature of heterogeneities in the fibres was evaluated using a Kratky (slit type) camera. The fibres were mounted parallel to the direction of the slit.

3.5. Auger electron spectroscopy

Auger electron spectroscopy was carried out using a Physical Electronics 590 A spectrometer. In determining the depth profiles, the samples were sputtered with argon ions, and the surface analysis was made with an electron beam about 0.8 μm diameter.

3.6. X-ray photoelectron spectroscopy

To investigate the form of boron present in the fibres, X-ray photoelectron spectroscopy was employed. Recognizing that the ionization energy of an element depends on its chemical state, a Physical Electronics 548 ESCA system was used to detect this shift of ionization energy for boron. The spatial resolution was 2 mm and the instrument was capable of resolving about 0.1% boron.

4. Results and discussion

4.1. Wide-angle X-ray diffraction

As indicated in Section 1 above, the effects of boron treatment in the production of carbon fibres have been mainly associated with increases in the elastic modulus. As also indicated above, the elastic modulus is considered to be a strong function of the orientation of the small graphite crystals in the fibres. The results of wide-angle X-ray scattering studies on a range of FMI-produced fibres processed under different conditions, as well as on Hercules HMPVA fibres, are summarized in Table III.

The values of the orientation function shown in Table III were evaluated from the (0 0 2) diffraction

TABLE III Structural parameters obtained from wide-angle X-ray diffraction

Fibre	Orientation function (f_{002})	Interplanar spacing d_{002} (nm)	Crystallite size (nm)
FMI 107-74	−0.460	0.347	3.3
FMI 098-374	−0.484	0.343	7.9
FMI 107-74A	−0.469	0.346	3.7
FMI 107-74-B	−0.459	0.346	3.5
FMI 098-85	−0.456	0.345	3.4
FMI 098-87	−0.464	0.347	3.4
FMI 098-93	−0.468	0.344	6.3
FMI 16-2	−0.484	0.343	6.1
FMI 21-4	−0.481	0.344	6.1
FMI 19-2	−0.481	0.343	5.9
FMI 21-8	−0.469	0.345	4.3
HMPVA	−0.474	0.345	5.0

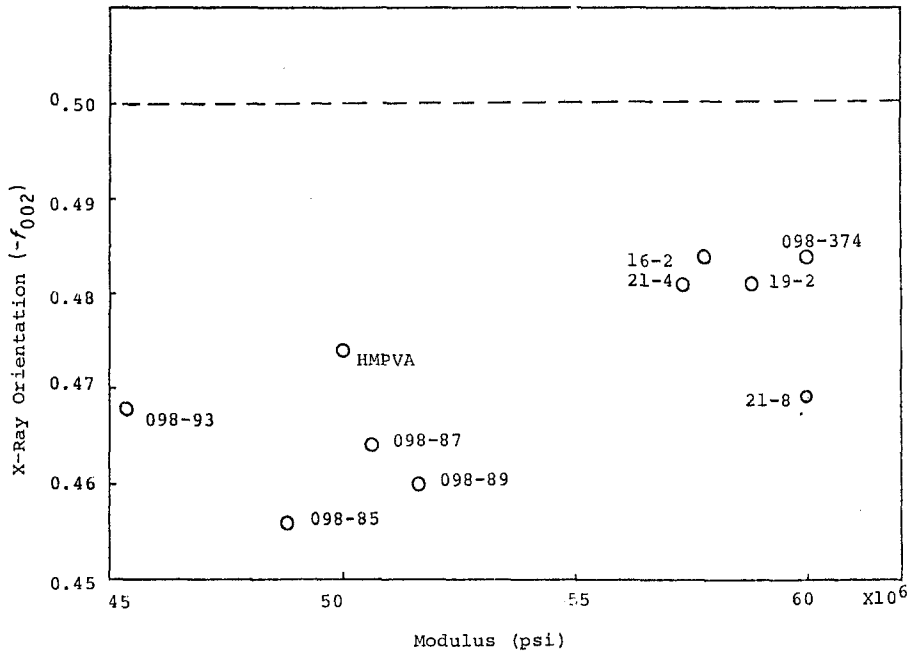

Figure 1 X-ray orientation plotted against the modulus of FMI fibres.

peak. In assessing these values, it should be noted that an orientation function of -0.5 indicates perfect alignment of the (0 0 2) planes perpendicular to the fibre axis. Also shown in the table are values of the (0 0 2) interplanar spacing, as well as the sizes of the coherently diffracting arrays (crystallite sizes). The last quantity was obtained from the breadth of the (0 0 2) diffraction peaks using the Scherrer formula.

Fig. 1 shows the variation of elastic modulus with orientation function for the FMI fibres. A general increase of modulus with crystal orientation is observed, although appreciable deviation from the average variation is seen in the results on the different fibres.

Comparing the results in Table III with the boron treatments of the respective fibres given in Table I, it is also seen that there is little correlation between any of the fibre characteristics obtainable from wide-angle X-ray diffraction and the boron treatment used in processing.

It is concluded, therefore, that the three structural characteristics obtained from wide-angle X-ray diffraction data (orientation function, crystallite size, and interplanar spacing) do not correlate well with either the mechanical properties of the fibres (strength and elastic modulus) or with the boron treatment used in preparing the fibres.

4.2. Scanning electron microscopy

4.2.1. External surfaces

The scanning electron micrographs shown in Figs 2a to c present representative views of the external surfaces of some of the fibres (all were examined in this way). The draw ridges seen in Fig. 2 are much more prominent in the FMI fibres than in the HMPVA fibres. The presence of these ridges is undoubtedly related to the processing conditions used by the respective manufactures, and could have important implications for the performance of the respective fibres in composites.

There was no clear distinction observed between the surface textures of boron-treated and non-boron-treated fibres. The fibres which were graphitized in atmospheres with carbonaceous species show deposits in some areas of a soot-like material which is anchored firmly to the fibres (e.g. Fig. 2c).

In some cases, defects could be seen in the surfaces of the fibres, as reported previously by others [4]. An example is designated by the arrow in Fig. 2a. No correlation could be established between the occurrence of such defects and the nature or even the use of treatment with boron in the furnace atmosphere.

4.2.2. Surfaces of polished cross sections

Figs 3a to e show representative polished cross sections of some FMI fibres. In addition to FMI fibres, observations were also carried out on the HMPVA, HMS, AS4 and Avco fibres. In the polished section of all of the FMI fibres as well as the HMPVA and HMS fibres, a distinct grain-like morphology was observed. No such grain-like features were seen in the polished cross-sectional surfaces of the AS4 and Avco fibres.

The mean sizes and standard deviations of mean size of the grain-like features in each of the fibres are presented in Table IV. It is seen that the mean size of the grain-like features did not vary greatly with the processing conditions: fibres prepared with different process histories by a given manufature (FMI) or fibres prepared by different manufactures exhibited comparable sizes of the grain-like features. Analysis was carried out of the possible relation between mean size of the grain-like features and the values of the orientation function determined from wide-angle X-ray scattering. These analyses compared the size of the grain-like features presented in Table IV with the values of the orientation function shown in Table II. No correlation was found between the two quantities.

It is interesting to note that the grain-like features are not seen in the polished cross-sectional surfaces of either of the high-strength fibres examined (see Figs 3c and d). While this observation could have important implications for the strength-limiting flaws in fibres

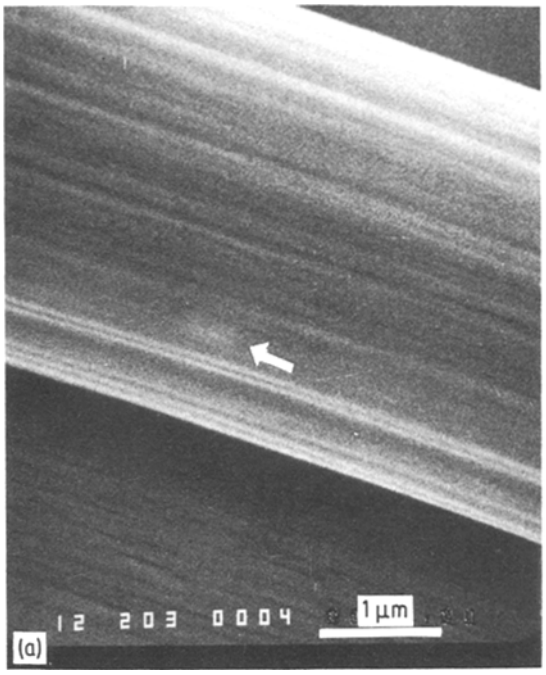

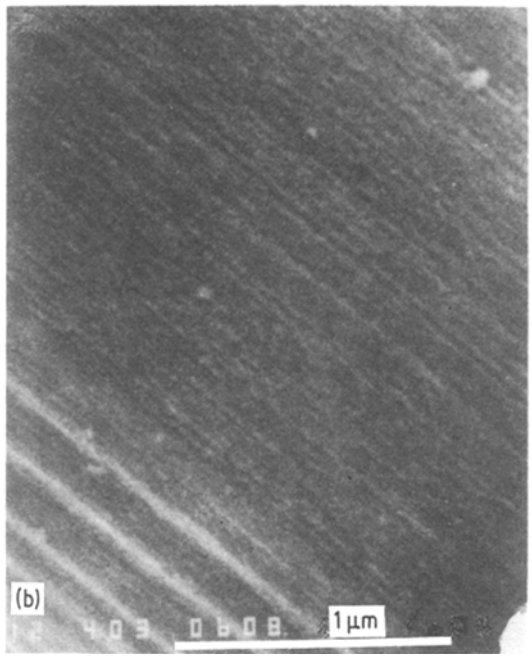

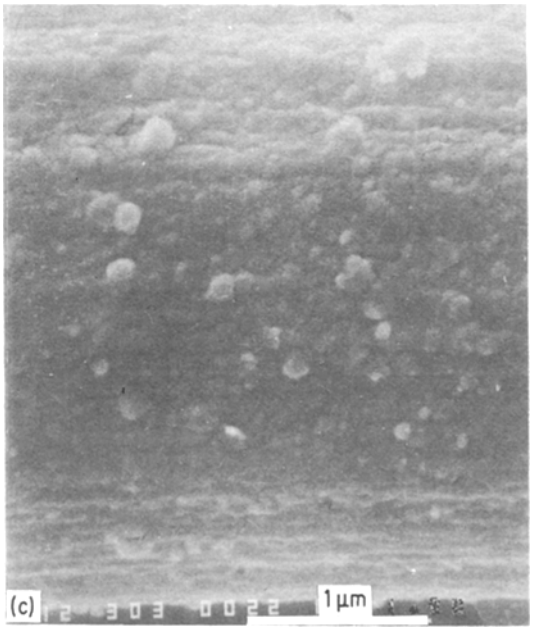

Figure 2 (a) Representative external surface of fibre FMI 098-93. Arrow shows an internal flaw close to the surface. (b) Representative external surface of fibre FMI 098-85. (c) Representative external surface of fibre FMI 098-89.

which break from internal flaws rather than from surface defects, the principles of fracture mechanics suggest that the flaws responsible for the observed modest strengths of the fibres are appreciably larger than the sizes of the grain-like features seen in the micrographs. The observed scale of the grain-like features may reflect the mechanical action of the polishing operation; and the presence or absence of the grain-like texture would then correspond with the observed demarcation between high strength and moderate strength fibres.

4.2.3. Fracture surfaces

Figs 4a to e show representative morphologies of the many dozens of fracture surfaces which were examined. In nearly all cases, a pronounced granularity was seen on the fracture surfaces. The size and even the form of the granularity was, however, different for different fibres, and was also in general larger than the size of the grain-like features seen on the polished surfaces.

The variation in size of the granular features was seen clearly in the micrographs for nearly all of the fibres. It is also observed that different fracture surfaces of the same fibre show quite different overall morphologies and apparent grain-like features (e.g. compare Figs 4a and b on fibre FMI 19–2). From these results, it seems clear that one cannot from such micrographs of fracture surfaces derive anything conclusive about the characteristics of the stacking of crystallites across the cross section of the fibre.

TABLE IV Mean sizes ($\bar{x}$) and standard deviations (σ) of granular features seen in polished cross sections

Fibre type	$\bar{x}$ (µm)	σ (µm)
FMI 107-24	0.032	0.005
FMI 098-374	0.026	0.008
FMI 107-74A	0.037	0.009
FMI 107-74B	0.031	0.004
FMI 098-85	0.028	0.004
FMI 098-87	0.034	0.006
FMI 098-89	0.029	0.006
FMI 098-91	0.032	0.005
FMI 098-93	0.039	0.007
FMI 16-2	0.042	0.010
FMI 21-4	0.048	0.009
FMI 19-2	0.028	0.008
FMI 21-8	0.028	0.006
FMPVA	0.031	0.005
FMS	0.039	0.007
AS4*	–	–
Avco*	–	–

*No granular features were observed.

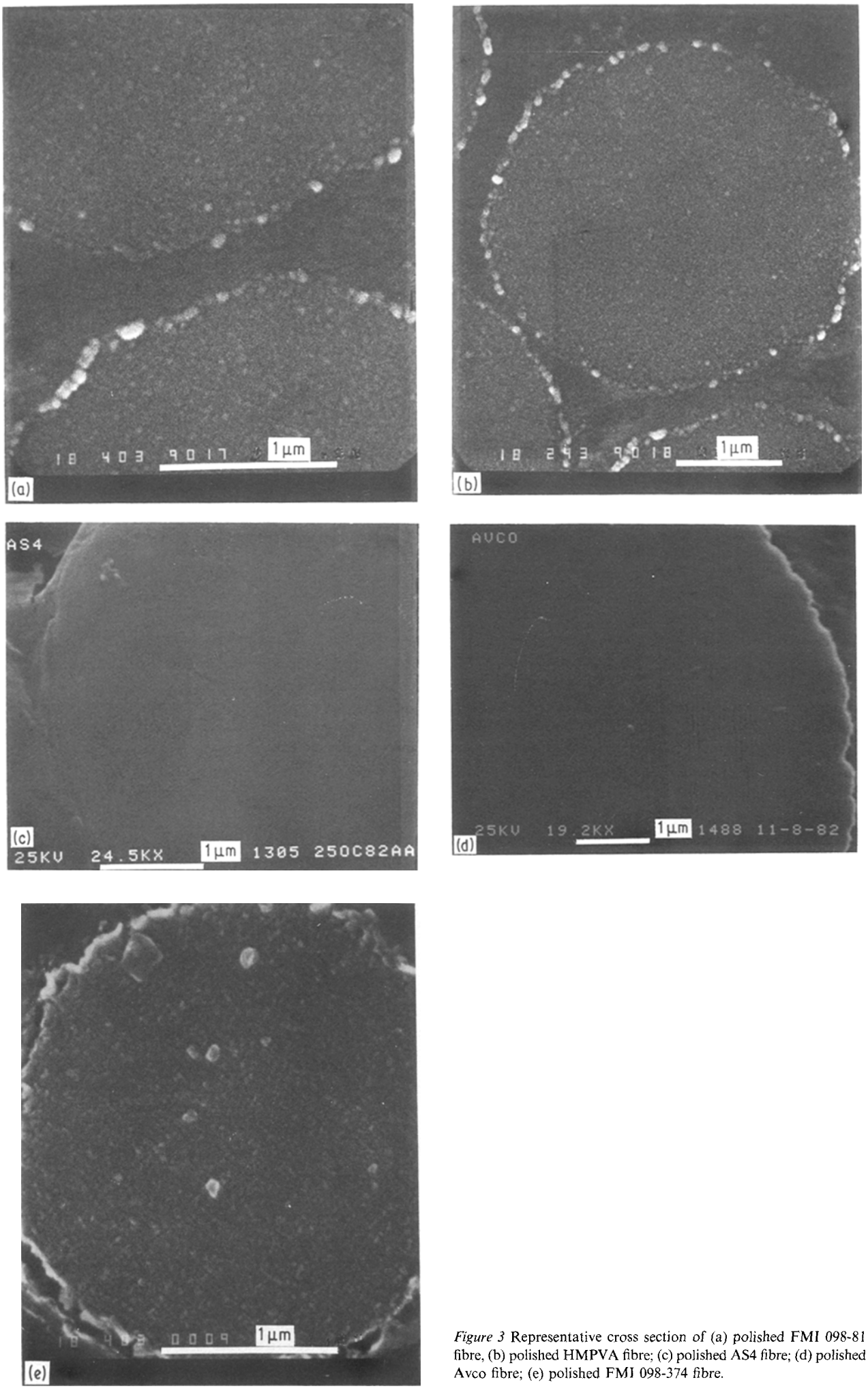

Figure 3 Representative cross section of (a) polished FMI 098-81 fibre, (b) polished HMPVA fibre; (c) polished AS4 fibre; (d) polished Avco fibre; (e) polished FMI 098-374 fibre.

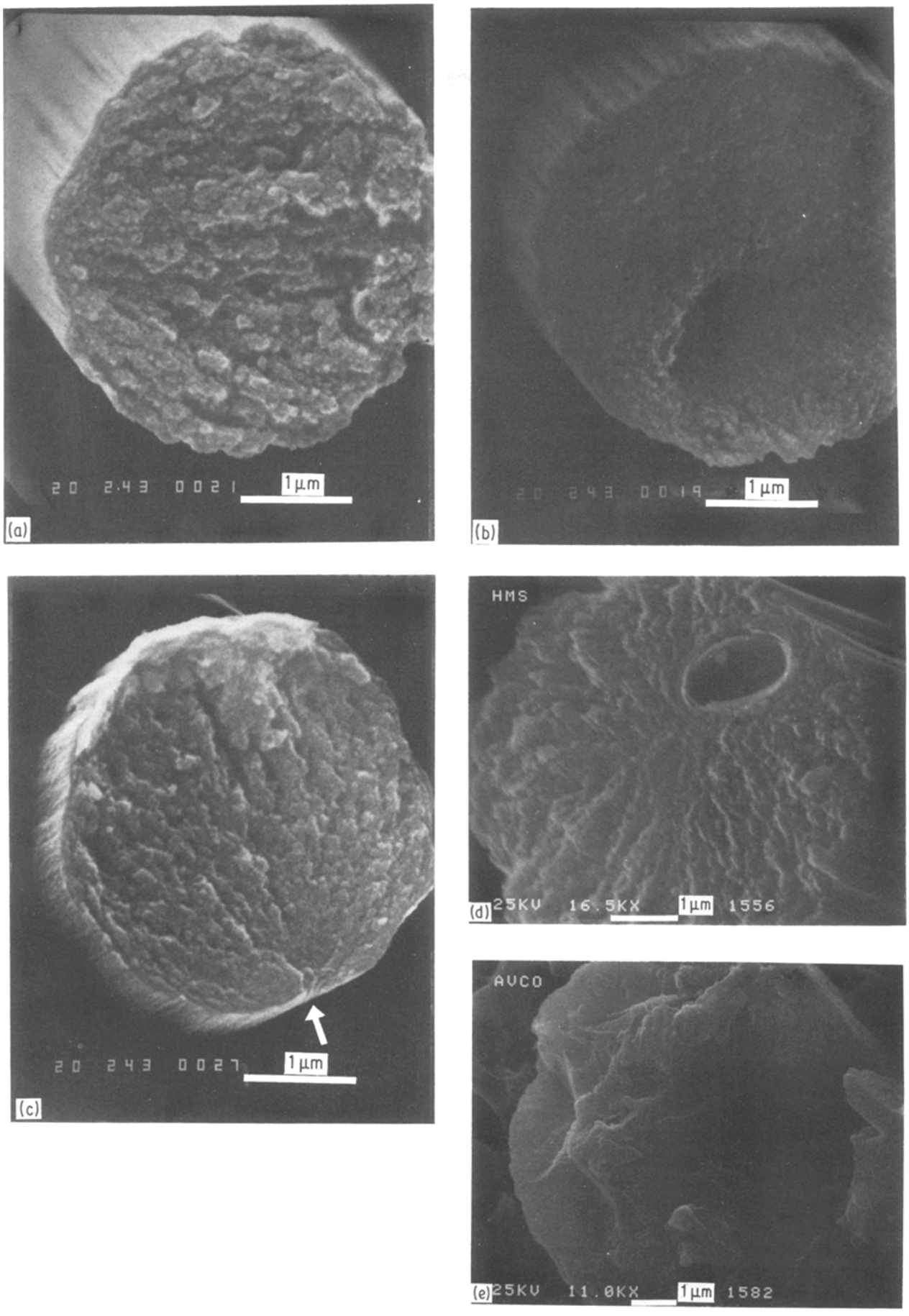

Figure 4 (a) Fracture morphology of FMI 19-2 fibre. Fracture initiated from a surface flaw. (b) Fracture morphology of FMI 19-2 fibre. Fracture initiated from an internal flaw. (c) Fracture surface morphology of FMI 21-4 fibre. Fracture initiated from a surface flaw. (d) Fracture morphology of a HMS fibre. Fracture initiated from an internal flaw. (e) Fracture morphology of an Avco fibre.

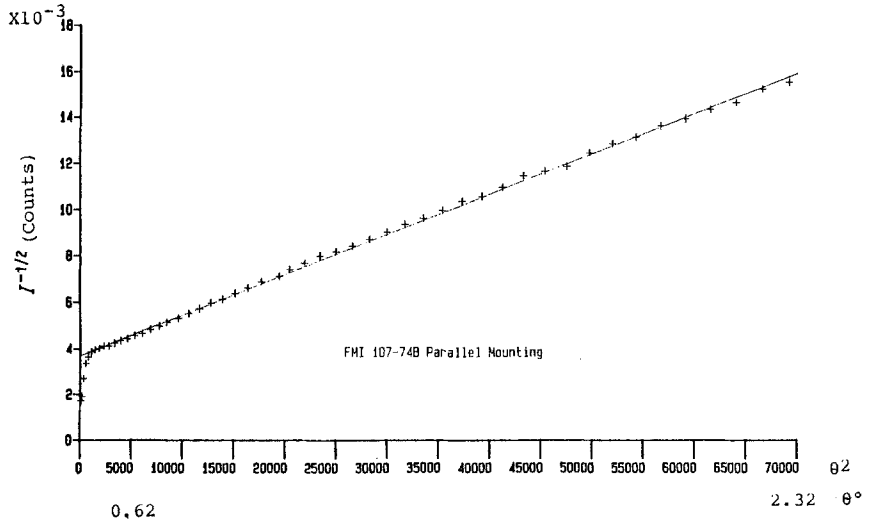

Figure 5 SAXS data plotted according to Debye Law.

Many of the fractures originated from flaws associated with the surfaces of the fibres. An example is shown by the arrow in Fig. 4c. In other cases, the fractures clearly originate from interior flaws (e.g. Fig. 4d). A clearly delineated sheath–core structure is seen in some fibres. In each case where it is clearly visible, the sheath is very small in thickness, and corresponds to a thin layer on the surface.

In exploring the differences in size of the grain-like features seen on the polished and fracture surfaces, it was recognized that in highly oriented organic fibres and films, fracture causes delamination along the orientation direction, giving rise to a fibrous appearance on a fine scale [25, 26]. It is suggested, therefore, that the granular features were likely produced during the process of fracture, with splitting occurring at the weaker boundaries between the structural features. This would also explain the absence of grain-like features in the high-strength fibres examined (see discussion above).

The dozens of observations of fracture surfaces indicate that neither the presence nor absence of boron in the furnace atmosphere during graphitization, nor the conditions of boron treatment, have a consistent effect on the features seen on the fracture surfaces. It was observed, however, that the boron-treated fibres exhibited a smaller propensity to fail from surface flaws than fibres not given such treatment. This point will be addressed further in the concluding discussion.

4.3. Small-angle X-ray scattering

Representative variations of the small-angle scattering (SAXS) intensity with scattering angle are presented in Figs 5a and b. The forms of the relations used to plot the small-angle data are based on the following considerations [27, 28]: for randomly distributed pores of random shape, the correlation function $c(r)$ between two points separated by a distance r is taken to be of the form

$$c(r) = \exp(-r/a) \quad (1)$$

where a is the correlation length for small angles. For small angles, the scattered intensity follows the Debye law:

$$\left(\frac{I_0}{I}\right)^{1/2} = 1 + \frac{16\pi^2}{\lambda^2}\theta^2 a^2 \quad (\theta \sim \sin\theta) \quad (2)$$

Here I is the scattered intensity at an angle θ, λ is the wavelength and I_0 is the intensity at $\theta = 0$. A graph of $I^{-1/2}$ against θ^2 should therefore give a straight line of positive slope. From the slopes of such plots, one can obtain the correlation length, a. The average chord length of carbon regions l_c is given by

$$l_c = a/(1 - D) \quad (3)$$

where D is the ratio of fibre density to the density of bulk graphite. Further, the average length of the pores, l_p, is given by

$$l_p = 2a \quad (4)$$

Values for the correlation length, the average chord length of the carbon regions and the average length of the pores are summarized in Table V, based on small-angle scattering data of the form shown in Fig. 5. As seen in the table, the average chord lengths of the carbon regions obtained from SAXS data are similar to values of the crystallite thickness obtained from wide-angle X-ray diffraction (compare with Table III).

In assessing the effect of boron treatment on the structural parameters obtained from SAXS (correlation length, average chord length of carbon regions and lengths of pores), the data shown in Table V do not show a pronounced dependence on boron treatment.

TABLE V Correlation length (a), chord length of carbon regions (l_c) and length of pore regions obtained from small-angle X-ray scattering data

Fibre	Density ($g\,cm^{-3}$)	a (nm)	l_p (nm)	l_c (nm)
098-374	1.96	0.86	1.72	7.88
107-74*	1.80	0.53	1.06	2.93
107-74B	1.83	0.53	1.06	3.15
21-8	1.81	0.52	1.04	2.93
107-74A*	1.80	0.47	0.94	2.58
098-85*	1.77	0.4	0.8	2.05

*Not treated with boron.

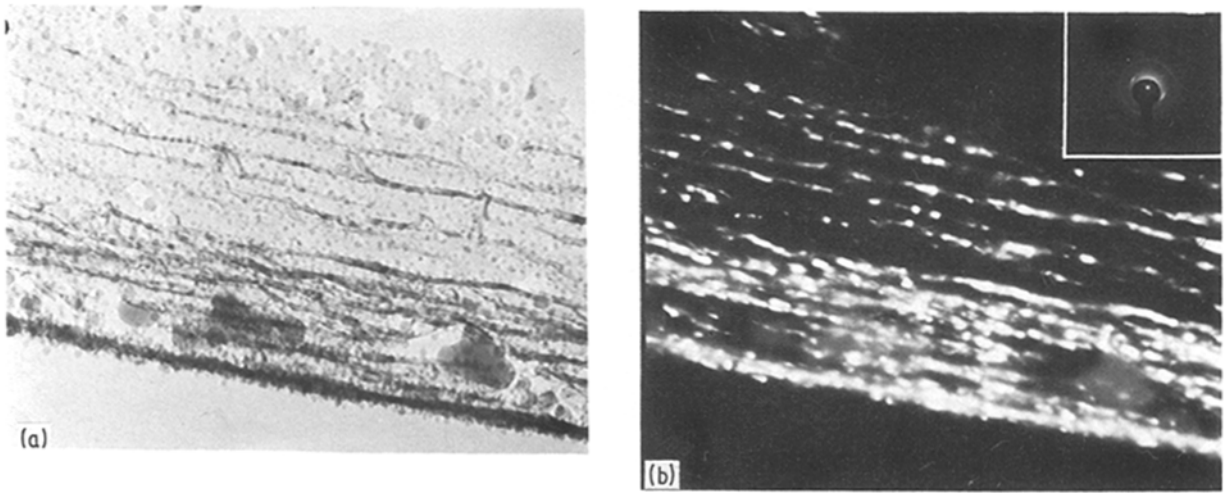

Figure 6 (a) Bright-field image of FMI 098-374 fibre edge. (b) Dark-field image of FMI 098-374 fibre edge. The insert shows the electron diffraction pattern of this fibre. Dark-field image was made from one of the intense spot of the (0 0 2) planes. (Innermost ring.)

4.4. Transmission electron microscopy

Direct transmission electron micrographs of fibres graphitized with boron in the furnace atmosphere showed the expected high degree of crystalline order in the near-surface regions. Fig. 6a shows a bright-field image of the near-edge (outer surface) region of a FMI 098-374 fibre. The regions of the edge and the immediate near-edge region are much more ordered as compared with the interior. It also appears that the soot on the outer surface (edge) of the fibre is also graphitized in the direction of the fibre axis. This is seen from the dark-field image corresponding to Fig. 6a, which is presented as Fig. 6b. In this case, a long exposure was given; and hence the contrast necessary for the observation of Moiré fringes is lost.

The degree of orientation in the near-edge regions appear to be greater in the case of boron-treated fibres than in fibres not provided with boron in the furnace atmosphere during graphitization. It seems therefore that the structural modifications due to boron treatment are confined largely to the region immediately adjacent to the surfaces of the fibres.

4.5. Auger electron spectroscopy

To examine the possible presence of boron in the boron-treated fibres – and if present, to determine the distribution of boron through the cross sections of the fibres – Auger spectroscopy was carried out. The average concentration of boron in the fibres was determined using raster scans with a raster size of 50 μm; while the distribution of boron through the fibres was determined by sputtering in from the fibre surfaces using Argon ions as the sputtering agent. The average rate of sputtering for the fibres was determined in separate measurements at about 15 nm min^{-1}.

Typical results of Auger spectroscopic analysis of boron-treated fibres are shown in Figs 7a and b. The results indicate a relatively high concentration of boron on the surface, but a concentration which decreases rapidly with increasing distance into the fibres. The horizontal dashed lines shown in the figures represent the detectability limit for analysis of the boron (imposed by the noise level). The data on fibre FMI 098-374 shown in Fig. 7a were collected using a beam spot size of about 2 μm rather than the beam size about 0.8 μm used with the other fibres. Since the diameter of the fibre was about 3 μm the data on FMI 098-374 may not be comparable with those on the other fibres. In all cases, the estimated concentrations of boron may be in error by as much as a few per cent.

Considering the data shown in Fig. 7b, it should be noted that the graphitization treatment of fibre FMI 21-4 was twice as long as that of fibre FMI 16-2 (see Table I). As might have been expected, fibre 21-4 shows a deeper penetration of boron into the bulk of the fibre. It should be noted that even in this case, the scale in the figure extends to only about 50 nm depth into the fibres.

Fibre FMI 107-74B was given an initial graphitization treatment in argon prior to the graphitization treatment in the boron-containing atmosphere. The initial graphitization treatment in argon apparently produced sufficient ordering in the immediate regions of the fibre surface to impede the diffusion of boron into the fibre during the subsequent boron treatment (compare the data on fibre FMI 107-74B with those on fibre FMI 16-2).

From boron mapping, the distribution of boron appears to be quite uniform on a large scale, but not on the scale of the spot size used in the Auger analyses (about 0.8 μm). Hence the compositional profiles shown in Fig. 7 should be taken as representative of the respective fibres, but not characteristic of every cross section through the fibres.

It should also be noted that in some cases heavy soot deposits were observed. In these cases, the surface composition of the heavy soot and the "clean" fibre surface were closely similar. It should also be noted that the two samples exhibiting long tails in Fig. 7a exhibit pronounced soot deposits. Both scans for fibre FMI 098-87 shown in the figure were, however, carried out in "clean" areas. The differences in the measured profiles between the two analyses was very likely associated with differences in the thickness of the respective soot deposits.

Taken *in toto*, the results of the Auger analysis

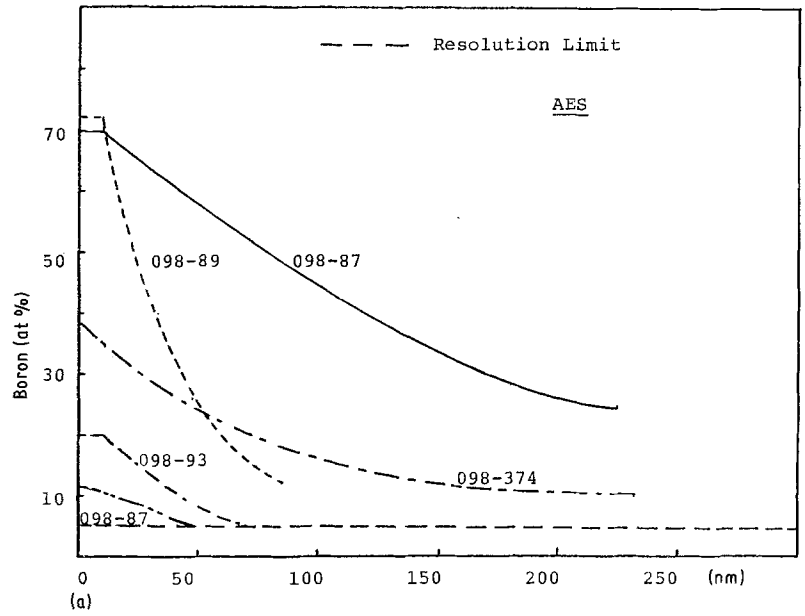

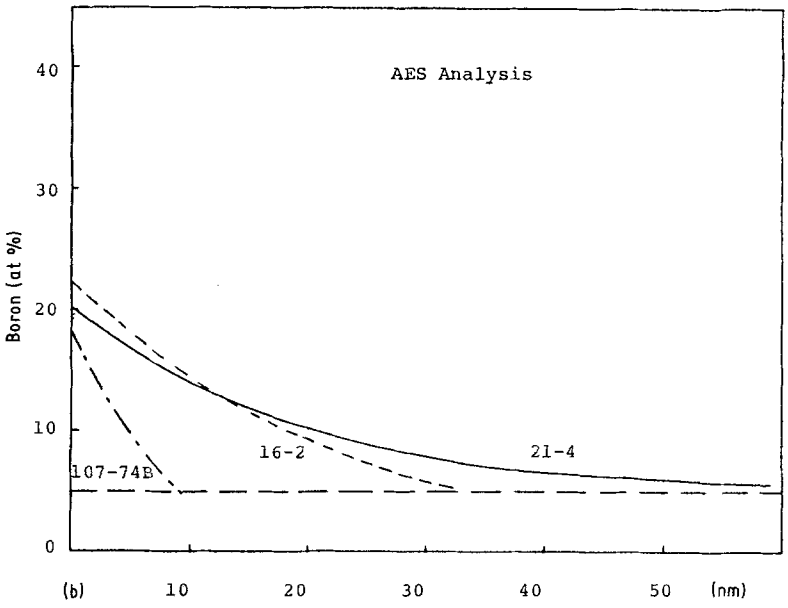

Figure 7 (a, b) Depth profiles of boron in FMI fibres by Auger electron spectroscopic analysis. (b) Depth profiles of boron in FMI fibres by Auger electron spectroscopic analysis.

indicate the presence of boron in all of the boron-treated fibres. The results also indicate that under the processing conditions employed in making the fibres which were studied, the boron is present only in the near-surface regions of the fibres (a few tens of nanometres in depth). Graphitization treatments with boron in the furnace atmosphere thus influence only the near-surface regions of the fibres, and would be expected to modify only those fibre properties which are surface sensitive. The most probable modifications would be healing of surface flaws by the formation of boron carbide which catalyses the graphitization process, and an enhanced degree of graphitization in the surface regions.

4.6. X-ray photoelectron spectroscopy (XPS)

To evaluate the chemical state of boron in the near-surface regions of boron-treated fibres, the technique of X-ray photoelectron spectroscopy was employed. This technique measures the binding energies of the electrons, which are sensitive to the oxidation state of an element. The binding energy difference between boron and boron carbide is, however, quite small; and standards were therefore used in the analysis. A boron standard was made using boron-coated tungsten filaments; and a sample of bulk boron carbide was obtained from the Norton Co. (Worcester, Massachusetts).

Fig. 8a and b shows the boron and carbon-peaks obtained from multiplex XPS scans on fibre FMI 21-4, as well as on the two standard materials (boron carbide and boron). It is seen in Fig. 8a that the boron peak for fibre FMI 21-4 corresponds more closely to boron in boron carbide than to elemental boron, although the data seem to suggest some admixture of the two forms.

The unalloyed carbon peak (C^{1S}) has been well documented at 284.8 eV. The carbon peak from fibre FMI 21-4 (Fig. 8b) is mainly associated with unalloyed carbon, undoubtedly from the adsorption of organic species onto the surface of the fibre. The shoulder toward higher binding energies in the data from the fibre does, however, suggest the presence of boron in the form of boron carbide.

It is concluded therefore that the boron in the boron-treated fibres is present in large part as a boron

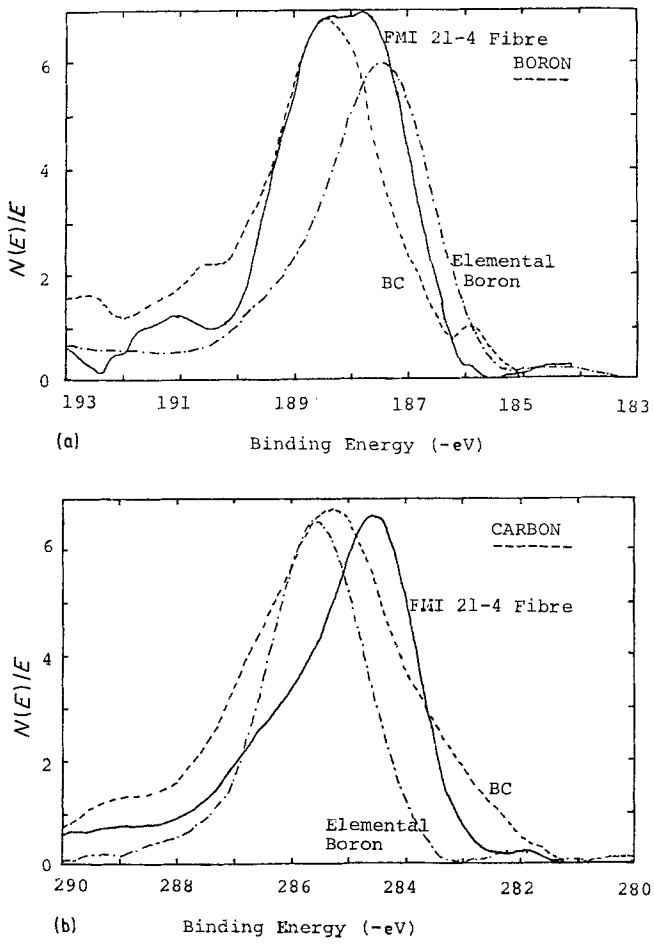

Figure 8 XPS analysis of the chemical shifts of (a) boron, (b) carbon.

carbide, but that some portion is also present as dissolved boron.

5. Discussion

At the time of initiation of the present work, significant improvements in mechanical properties had been observed for boron-treated carbon fibres; but in some cases at least, the presence of boron in the resulting fibres could not be observed. It was also uncertain how the boron could function to produce the observed improvements in properties; and several models had been advanced to this end, some of which appealed to structural changes in the bulk of the fibres.

The results of the present investigation have clarified the situation, as seen from the following conclusions.

1. The presence of boron in the furnace atmosphere does *not* affect the important structural features of the bulk of the fibres. This was apparent from comparing boron-treated and untreated fibres with respect to crystallite size, (0 0 2) interplanar spacing (and hence perfection of the graphite crystals), degrees of orientation, chord length of the carbon regions, and radii of the pores.

2. The presence of boron in boron-treated fibres has been unequivocally documented. For the FMI fibres investigated, the added boron is largely confined to the near-surface regions (typically within a few tens of nanometres of the fibre surface).

3. Such boron treatments should therefore be effective in modifying properties of the fibres which are sensitive to surface characteristics. Most notable among these is the strength in cases where the strength is limited by surface flaws. The overall moduli of the fibres should be less affected by boron treatment, although notable increases in the moduli of the near-surface regions are expected.

4. A large fraction of the boron is present as boron carbide; and such carbide formation seems important to the observed improvements in strength. It is noteworthy in this regard that the largest improvements in strength were obtained in cases where *both* carbon and boron were present in the furnace atmosphere during graphitization.

It is not possible from the present results to draw inferences about the possible role of dissolved boron in modifying the structure and properties of the bulk of the fibres, if processing conditions were employed which provide boron throughout the cross section of the fibres. By analogy with the present results, it seems that the formation of boron carbide within the fibres could further modify the strength and modulus. It is difficult to believe, however, that the large voids seen in an unexpectedly large fraction of the fibres (a few per cent) would be affected by any boron treatment. It seems advisable to direct attention to the elimination of such voids by other modifications of precursor chemistry and processing.

Acknowledgement

Financial support for the present work was provided by the US Army Mobility Equipment Research and Development Command. This support is gratefully acknowledged.

References

1. J. W. JOHNSON, *Polymer Preprints Amer. Chem. Soc.* **9** (1968) 1316.
2. J. W. JOHNSON and D. J. THORNE, *Carbon* **7** (1969) 659.
3. D. SHARP, S. G. BURNAY, J. R. MATTHEWS and E. A. HARPER, International Conference on Carbon Fibres (The Plastics Institute, London, 1974).
4. D. J. THORNE, Third Conference on Industrial Carbons and Graphite, London, 1970 (Society of Chemical Industries, London, 1971) p. 463.
5. W. WHITNEY and R. M. KIMMEL, *Nature Phys. Sec.* **237** (1972) 93.
6. R. MORETON and W. WATT, *Carbon* **12** (1974) 543.
7. A. OYA and H. MARSH, *J. Mater. Sci.* **17** (1982) 309.
8. A. OYA and S. OTANI, *Carbon* **17** (1979) 131.
9. T. ISHIKAWA and S. YOSHIZAWA, *Kogyo Kagaku Zasshi* **66** (1963) 933.
10. W. WEISWEILER, S. SUBRAMANIAN and B. TERWIESCH, *Carbon* **9** (1971) 755.
11. J. GILLOT, B. LUX, P. CORNUAULT and C. F. du CHAFFAUT, *Ber. Dtsch. Keram. Ges.* **45** (1968) 224.
12. C. YOKOKAWA, K. HOSOKAWA and Y. TAKEGAMI, *Carbon* **4** (1966) 459.
13. *Idem, ibid.* **5** (1967) 475.
14. A. OYA, R. YAMASHITA and S. OTANI, *Fuel* **58** (1967) 495.
15. R. M. MAYER, 11th Biennial Conference on Carbon (The American Carbon Committee, 1973) p. 26.
16. W. H. REIGER, Proceedings of the Third Conference on Industrial Carbon and Graphite, London, 1970 (Society of Chemical Industries, London, 1971) p. 126.
17. S. MARINKOVIC, C. SUZNJEVIC and I. DEZAROV, *Carbon* **7** (1969) 185.
18. W. V. KOTLENSKY, *ibid.* **5** (1967) 409.
19. R. J. DIEFENDORF, French Patent 1 552 357 (1969).
20. H. M. EZEKIEL, 11th Biennial Conference on Carbon, Gatlinberg, 1973 (The American Carbon Committee, Abstracts, 1973) p. 267.
21. S. ALLEN, G. A. COOPER and R. M. MAYER, *Nature* **224** (1969) 684.
22. R. PEPPER, D. NELSON, D. JARMON and J. HOTHAM, Final Technical Report on Improved Graphite Fiber, Contract No. DAAK70-77-C-0-0155, US Army Mobility Equipment Research and Development Command (1978).
23. E. J. WATTS, *Metallogr.* **9** (1976) 43.
24. D. J. JOHNSON and D. CRAWFORD, *J. Mater. Sci.* **8** (1973) 286.
25. A. PETERLIN, *Polym. Eng. Sci.* **17** (1977) 183.
26. *Idem, J. Macromol. Sci. Phys.* **B7(4)** (1973) 705.
27. A. FOURDEUX, R. PERRET and W. RULAND, International Carbon Fiber Conference (The Plastics Institute, London 1971) p. 59.
28. W. RULAND and R. PERRET, *J. Appl. Cryst.* **2** (1969) 209.

Received 12 April
and accepted 30 May 1985